ACI Materials Journal, Vol. 92, No. 3
May-June 1995, pp. 276-285.

TENSILE AND BOND PROPERTIES OF GFRP REBARS

by L. Javier Malvar

ABSTRACT

The bond characteristics of four different types of glass fiber reinforced plastic (GFRP) rebars with different surface deformations were analyzed experimentally. Local bond stress-slip data, as well as bond stress-radial deformation data, needed for constitutive modeling of the interface mechanics, were obtained for varying levels of confining pressure. In addition to bond stress and slip, radial stress and radial deformation were considered fundamental variables needed to provide for configuration-independent relationships. Each test specimen consisted of a #6 GFRP rebar embedded in a 3-inch (76 mm) diameter, 4-inch (102 mm) long cracked concrete cylinder subjected to a controlled, constant amount of confining axisymmetric radial pressure. Only 2.625 inches (67 mm, i.e. the equivalent of 5 steel bar lugs) of contact were allowed between the bar and the concrete. For each rebar type bond stress-slip and bond stress-radial deformation relationships were obtained for five levels of confining axisymmetric radial pressure. It was found that small surface indentations were sufficient to yield bond strengths comparable to that of steel bars. Effects of the deformations on tensile properties were addressed. It was also shown that radial pressure is an important parameter which can increase the bond strength threefold.

Keywords: bond (concrete to reinforcement); concrete; FRP; composites; E-glass

L. Javier Malvar, MACI, is an Assistant Research Engineer, Civil Engineering Department, University of California, Davis, CA 95616. He has conducted research on fracture mechanics, finite element modeling and experimental analysis of concrete and reinforced concrete structures at the Naval Facilities Engineering Engineering Service Center, Port Hueneme, CA.

INTRODUCTION

Extensive and costly condition assessment, repair and rehabilitation programs are under way to extend the service life of reinforced concrete structures. The main cause of deterioration is the corrosion of the steel reinforcement exposed to marine environment and aggressive agents such as deicing salts for bridges and pavements. To prevent this corrosion, galvanized and epoxy coated bars are currently being used and investigated [1-4], with mixed results [2]. A more recent alternative is the use of fiber reinforced plastic (FRP) bars which have excellent corrosion resistance and mechanical properties similar to steel [5,6]. FRP rebars, tendons and grating have already been used in waterfront structures and bridges [6-11].

A concern with FRP rebars, as well as epoxy coated rebars, is the behavior of the interface between rebar and concrete [3,12-19]. The objectives of the present study are to investigate mechanical properties and bond-slip behavior of four commercially available FRP rebars. For each FRP rebar type, up to eight tensile tests are carried out and bond stress-slip constitutive relationships are experimentally determined. This latter data is obtained as a family of bond stress-slip curves for five levels of constant radial confining stress. In addition, bond stress-radial deformation curves are obtained which characterize the radial expansion at the interface.

RESEARCH SIGNIFICANCE

The acceptance of FRP rebar in structural engineering has been inhibited partly due to the lack of design criteria, particularly with regard to bond [20,21]. One reason for the lack of design criteria for bond is the lack of standards for the bar deformations geometry and bar composition. Comparison of bond properties of various types of deformations is a first step in the determination of optimum deformation geometry.

The determination of constitutive bond stress-slip relationships is useful for mathematical or numerical modeling of reinforced concrete structural behavior. In particular, these models can be used to determine anchorage requirements for reinforcing bars without need for extensive testing.

TENSILE AND BOND TESTS FOR FRP REBARS

Rebar Types

Four commercially available FRP rebars types with different deformations are considered (Figure 1). All four are 3/4-inch (19 mm) diameter bars composed of pultruded E-glass fibers with a fiber volume fraction of 45% (60% by weight) or more, embedded in a vinyl ester or polyester resin matrix. For each one Table 1 reports the deformations spacing in inches and as a fraction of the nominal diameter ∅, and the coefficient of variation. For steel bars, the maximum deformation's spacing is 0.7 ∅, i.e. 0.525 inches (13 mm) for a #6 bar [22]. Table 1 also indicates the deformations height (or the indentations depth) in inches and as a fraction of the diameter. The deformations height (or indentation depth) is measured as the difference between the bar

radius at a deformation and the radius at midpoint between that deformation and the next one. In addition each rebar type presents the following characteristics:

1) Type A. These bars have an external helicoidal tow which both provides a protruding deformation and a small indentation of the bar surface. An outer layer consisting exclusively of matrix material is provided around the fibers for additional protection. The deformations width was about 0.125 in. (3.2 mm), yielding a clear deformation spacing of 0.595 in. (15 mm).

2) Type B. During the fabrication of these bars the surface tow is stressed so that indentations are obtained instead of deformations. These bars showed a large variation of cross section which was expected to yield a variation in mechanical properties. Large variations in the surface indentations were apparent as well.

3) Type C. These bars have the surface tow glued to the exterior of the bar to provide only surface deformations. Fibers in the bar itself are perfectly straight.

4) Type D. Here an indentation similar to the one in type B is provided. These bars appear to have an outer veil to protect the glass fibers.

Tensile Tests

For each type, five tensile tests following ASTM D3916-84 [23] were first conducted to determine the secant modulus of elasticity at 24 ksi (165 MPa), the ultimate stress and the ultimate strain. The secant modulus was measured since it is expected that a working stress approach would be used in design, with allowable stresses between 18 and 30 ksi (124 and 207 MPa). Elongation measurements were taken using two LVDT's on either side of each bar, attached via two clamps spaced an average of 13 inches (330 mm). Total specimen length was 42 inches (1.07 m) with a clear spacing between grips of about 28 inches (0.7 m).

It was decided that these tests, which use an actual bar specimen, would be more representative than the ones under ASTM D638-90 [24] which requires a machined down specimen. The shortcomings of using a machined specimen are that the effects of indentations and specimen size on tensile strength cannot be evaluated, and the bar cross-sectional area may not be easily determined. The shortcomings of using an undisturbed bar specimen are related to grip effects. To alleviate these grip effects, three additional tensile tests were conducted for Types A and C. In these tests, specially designed grips consisting of four aluminum blocks bolted together were used and new values for the ultimate stresses were obtained.

Bond Tests

The objective of these tests was to determine configuration-independent, local bond stress-slip data for use in constitutive material models. Typically bond stress-slip curves are derived from pull-out tests, or other more complex setups, without regard for the lateral confinement exerted by the particular setup. As a result very disparate curves have been obtained which are only representative of the particular setup. If the lateral confinement is taken into account, a family of curves can be obtained, which could be used with any other configuration.

Similar tests have already been carried out for steel bars [25-27] yielding general bond stress-slip relationships which were successfully used in predicting a variety of well known results [28-30]. For FRP bars, the bond strength is more affected by the low transverse stiffness which is itself mostly dependent on the matrix material.

The specimen used is shown in Figure 2. It consists of a 3-inch (76 mm) diameter, 4-inch (102 mm) long concrete cylinder surrounding an FRP bar. Only 2.625 in. (67 mm) of the bar are actually in contact with the concrete, contact being prevented in the rest of the specimen via silicone-rubber spacers. The outer concrete surface is surrounded by a split, threaded steel pipe which carries the pullout force via shear stresses (Figure 3). The pipe is split into 8 strips in order to offer no lateral resistance. The concrete cylinder is actually cast in place against the pipe threads. Casting was carried out with the specimen placed vertically.

The radial confining pressure on the specimen is applied via a thin ring which surrounds the portion of pipe containing the concrete cylinder. A hydraulic jack with an adjustable relief valve closed the ring with a constant force during the test. In this way the longitudinal reaction and the radial confinement can be both controlled and measured independently of each other.

Concrete mix proportions were 1:3.02:1.35 for cement, sand and 3/8-inch gravel, respectively. The water-cement ratio was 0.55. Three uniaxial unconfined compressive tests at 28 days on three 6-inch tall, 3-inch diameter cylinders yielded a compressive strength of 4220 psi (29 MPa). Three tensile splitting tests on the same specimen size yielded a tensile strength of 405 psi (2.8 MPa).

On the loaded end, two LVDT's were clamped to the bar and measured the relative displacement of the outer concrete surface, i.e. the pipe. They were diametrically opposed to compensate for any rotation. A third LVDT was located inside the pipe and measured the relative displacement (slip) between the pipe and the unloaded end of the bar. Finally a fourth LVDT measured the opening of the confining ring. This was later translated into a radial deformation. The apparatus was installed in a MTS testing machine. The MTS load cell provided pullout load measurements. Bond stresses were calculated by dividing pullout loads by the contact area between bar and concrete.

Prior to each test the concrete cylinder was precracked by setting a bar surface pressure of 500 psi (3.4 MPa) and pulling on the bar until longitudinal splitting would occur. The specimen was then unloaded. After cracking, the confining pressure at the bar surface was set at either 500, 1500, 2500, 3500 or 4500 psi (3.4, 10.3, 17.2, 24.1 or 31 MPa) and kept constant during the remaining of the test (these E-glass composites have transverse compressive strengths around 20 ksi, or 138 MPa). After cracking (and assuming that the cracks are open) all the pressure from the confining ring is transferred to the bar. All tests were carried out in displacement control.

EXPERIMENTAL RESULTS

Tensile Tests Results

For each type Table 2 shows the average properties obtained. The modulus of elasticity indicated is the secant modulus at a stress of 24 ksi (166 MPa). Ultimate stresses are obtained by dividing ultimate loads by the nominal cross section. Coefficients of variation are also included. For each type the following observations are pertinent:

1) Type A. These bars have an additional layer consisting exclusively of matrix material around the fibers. This layer would tend to separate and initiate the bar failure, usually close to the grips. Subsequent to this separation (which resulted in a sudden stress drop) the bars could be reloaded to loads close to the ultimate. In all five tests longitudinal splitting of the bar was observed which could be caused by a weak fibre-matrix interface [31]. Additional tests using the special grips showed reduced grip effects and yielded higher ultimate stress values.

2) Type B. The indentations produced sharp kinks in the longitudinal bar fibers. Bar failure was initiated by cracking at the kinks.

3) Type C. During the tests it was observed that the deformations would break and separate from the bar surface. In two cases, failure initiated at the grips. In all tests longitudinal splitting of the bar was observed. Successive tests with the special grips showed a significant increase in the ultimate stress, to 103 ksi (710 MPa). Previous tests on these bars following ASTM D638 yielded an average ultimate stress of 100 ksi (690 MPa) and an elastic modulus of 6.1 Msi (42 GPa) [17].

4) Type D. As in type B, bar failure usually initiated at the indentations. Previous tests on two 3/4-inch (19 mm) coupons following ASTM D638 were reported to yield ultimate stresses of 77.6 and 84.6 ksi (535 and 583 MPa) similar to the current average value [32].

Bond Tests Results : Complete Bond Stress-Slip Curves

Tests 1 through 5 for each bar type correspond to confining pressures at the bar surface of 500 through 4500 psi (3.4 through 31 MPa) in 1000 psi (6.9 MPa) increments, as mentioned earlier. The slip mentioned in this section is the average measurement of the two LVDT's located on the loaded end of the bar. This measurement was corrected for the unbonded length of rebar and the gage offset. Figure 4 shows the longitudinal cracks for all four types under a confining stress of 500 psi (3.4 MPa). Figure 5 shows the complete bond stress versus loaded-end slip response. If the slip at the unloaded end were to be included in Figure 5, it could hardly be differentiated from the loaded end slip (both slips only differ initially as explained in the next section.

1) Type A. In test 5 of type A (missing from Figure 5a), the concrete cylinder appeared weaker and those results were discarded. Although the concrete specimen was subjected to a confining pressure of 4500 psi (31 MPa) at the bar surface in excess of the uniaxial compressive strength, in most cases this did not result in crushing (due to the multiaxial confinement). The response is qualitatively similar to that of steel rebars [25-27] in that the bond stress peaks rapidly, then decays smoothly up to a slip approximately equal to the clear deformation spacing, and finally remains constant thereafter. Bond strength increased threefold with confinement. The concrete in front of the deformations was crushed and sheared, but the bar surface was damaged as well, reflecting the relatively low shear strength of the composite.

2) Type B. Bond strength also increased threefold with confining pressure. A large scatter was present: for test 5 the bar had much greater indentations yielding an unexpectedly high bond strength, and peak slips varied significantly

3) Type C. In these tests the concrete cylinder never split, so most of the confining pressure was carried by the concrete cylinder as hoop stress. Consequently the response is almost not affected by confinement. The response exhibits a high initial adhesion followed by a constant bond stress for all five tests. For this type, it was observed that the deformations initially glued to the bar would break and separate from the bar during the test [33]. Subsequently bond resistance was only provided by friction between the bar itself and the concrete. Since the adhesion between bar and deformations can be variable and is not easily determined, this type of deformation is not recommended.

4) Type D. In two of these specimens the protective veil was sheared off the bar surface. Bond strength increased smoothly up to fourfold with increasing confinement. Bond stresses peaked at relatively high slips and remained high thereafter. This is an advantage since it allows for more stress redistribution in the structure and more energy dissipation. This indentation geometry appeared most efficient in terms of bond response.

5) Confinement Effects on Bond Strength. Figure 6 compares these results with previous data obtained for steel rebars [25-27]. It is seen that the maximum normalized bond strengths (bond strength/tensile strength) obtained are similar in magnitude (between 4 and 5) although they are obtained for higher confinement values (confining stress/tensile strength). For a given confinement, the bond strength developed by a steel bar is between 1.2 and 1.5 times higher than that of the equivalent FRP bar.

6) Effect of Indentation Depth. Two additional tests for types B and D were run as a means of evaluating the effects of indentation depth on the results.

For type B, a bar was chosen with a low indentation depth of 0.022 in. (0.56 mm). This test (3a) was carried out at a confinement of 2500 psi (17.2 MPa) to compare with test 3 where the bar had an average indentation depth of 0.057 in. or 1.45 mm (test 5 indentation depth was 0.088 in. or 2.24 mm). Test 3a showed a bond strength decrease of about 18% when compared to test 3 [33].

Similarly for type D, a second test (2a) was carried out at a confinement of 1500 psi (10.3 MPa). The bar in test 2a had an indentation depth of 0.051 in. (1.3 mm) versus 0.071 in. (1.8 mm) for test 2. Test 2a showed a corresponding decrease in bond strength of 16%.

Although deeper indentations may yield higher bond strengths, they also promote lower tensile strengths due to the resulting kinks in the fibers. An outer, helicoidal layer of fibers (as in a cable) could yield deformations without sharp kinks.

Bond Tests Results : Initial Bond Stress-Slip Curves

Upon starting the loading, the two LVDT's on the loaded end of the rebar start measuring displacement, however, the internal LVDT on the unloaded end does not record any movement for some time. During this initial phase the slip is non-uniform within the 5 lug test section of the

rebar. This is in contrast with the end of the test where all three LVDT's record practically equal slips. Reference 29 shows the evolution of the slip distribution along the test length. For the beginning of the loading it indicates that the average slip within the test length is approximately equal to:

$$\text{Average initial slip} = (2s_2 + s_1)/3$$

Where: s_1 = average slip from two loaded end LVDT's
s_2 = slip from unloaded end (internal) LVDT.

In all cases the initial bond stress-average slip curves showed some adhesion, i.e. a bond stress at zero average slip, between 100 and 300 psi (0.7 and 2.1 MPa). Beyond this adhesion, the slope of the curve appears to increase with higher confinement [33].

Bond Tests Results : Bond Stress-Radial Displacement Curves

Upon first loading the rebar deformations exert radial pressures against the surrounding concrete until the latter splits longitudinally. If external confinement is provided (as in the present case), the rebar tends to slowly open the concrete cracks until enough space is created for the deformations to advance, via a combination of sliding, concrete crushing, and superficial bar damage. Eventually, after enough combined damage has taken place, a radial contraction may occur [25-27]. To capture this dilation/contraction the ring opening was measured, which is converted to a radial displacement at the outer surface of the concrete cylinder specimen. The bond stress versus radial displacement curves obtained are shown in Figure 7.

For each rebar type the following was observed:

1) Type A. A response qualitatively similar to that of steel rebars [25-27] is obtained, where radial dilation takes place, mainly past the peak stress, then a fairly constant maximum opening is reached, usually followed by a contraction. The contraction is most visible in test 1, whereas the constant maximum opening is more obvious in tests 2 and 3. The maximum dilation reached decreases rapidly with increasing confining pressure. In test 4, the external pressure is high enough to prevent any dilation and allow only for some contraction at the end of the test. For this, and higher, external pressures the longitudinal cracks do not open and some of the confinement is carried via hoop stresses. ond failure occurs via lateral contraction of the bar and superficial bar damage, in addition to crushing/shearing of the concrete in front of the deformations. It is expected that it will not be possible to significantly exceed the bond strength attained by further increasing the external confinement.

2) Type B. A similar response is obtained. Larger dilations are obtained due to the presence of large indentation depths.

3) Type C. No dilation is apparent, due to the fact that the concrete cylinders never split.

4) Type D. No contraction is apparent at the end of the tests, possibly due to the limited slip attained (relative to the indentation spacing). Some scatter is present as shown by the fact that

test 3 has a greater maximum dilation that test 2No dilation is present for the higher confining pressures.

ANALYTICAL MONOTONIC ENVELOPE

An analytical expression for the monotonic bond stress-slip curve would be useful to extend the present results to situations with generic confinement and different concrete strength. This expression in derived in a two step procedure. First the peak on the bond stress-slip curve is defined as a function of confinement as follows:

$$\tau_m/f_t = A + B\,(1 - e^{-C\sigma/f_t})$$

$$\delta_m/\varnothing = D + E\,\sigma/f_t$$

where:

τ_m	=	bond strength (peak bond stress)
σ	=	confining axisymmetric radial pressure
f_t	=	tensile strength
δ_m	=	slip at peak bond stress
$\varnothing$	=	nominal bar diameter
A,B,C,D,E	=	non-dimensional empirical constants for each bar type

Second, the complete normalized bond stress-slip curve can be expressed as:

$$\tau = \tau_m \frac{F\,(\delta/\delta_m) + (G - 1)\,(\delta/\delta_m)^2}{1 + (F - 2)\,(\delta/\delta_m) + G\,(\delta/\delta_m)^2}$$

where: F,G = non-dimensional empirical constants for each bar type.

The constants were evaluated for bar types A and D (types B and C were not considered, B due to the scatter, and C due to the constant response), and also for the two types of steel bars from references 25-27 (with lugs inclined at 68° and 90° respectively with the longitudinal axis) and are reported in Table 3. These analytical fits are compared to the actual data for Type A in Figure 8.

The proposed empirical formulas are limited to the ranges of pressures tested. They are useful for calibration of simple numerical models which can compute the bond stress-slip response as a function of radial stress. This may be accomplished via bond-link, or node-tie elements, which can be viewed as two orthogonal springs connecting two nodes with identical coordinates [34]. However, a more complete representation of bond phenomena should also be able to reproduce the radial dilation which accompanies slip, e.g. using interface elements [28-30].

CONCLUSIONS

Tensile and bond properties for four types of FRP rebar with different deformation patterns were analyzed experimentally. Local bond stress-slip and bond stress-radial displacement curves were obtained for various levels of axisymmetric radial confining pressure. It was found that:

1) Tensile tests using actual bar specimens (following ASTM D3916) instead of coupons showed that deep indentations and the resulting kinks in the longitudinal fibers will reduce bar strength. Grip effects were found using the ASTM-D3916 setup which were mitigated by using special grips. Significant variations in dimensions and properties were apparent for some rebars.

2) For the 3/4-inch (19 mm) diameter bars tested, the ultimate strengths varied from 65 to 103 ksi (448 to 710 MPa) and the moduli of elasticity from 4.1 to 6.9 Msi (28 to 48 MPa).

3) Small surface deformations, about 5.4% of the nominal rebar diameter (i.e. similar to that of steel), are sufficient to yield maximum bond stresses up to five times the concrete tensile strength, similar to that obtained with steel rebars. Either surface deformations or indentations obtained by stressing an external helicoidal strand are acceptable for bond purposes. Deformations just glued to the surface are not recommended since they may become unbonded and thereafter fail to provide any bond per se.

4) For one same amount of confinement, the bond strength for a steel bar is, on average, 1.2 to 1.5 times greater than the bond strength for a FRP bar (for the cases studied).

5) Large variations in the indentation depths resulted in large variations in bond strength.

6) Bond strength can usually be increased threefold by increasing confining pressure.

ACKNOWLEDGMENT

Funding and facilities for the present study were provided by the Naval Facilities Engineering Service Center (formerly Naval Civil Engineering Laboratory), Port Hueneme, CA. Support provided by Dr. T.A. Shugar and Mr. Gary Neal is gratefully acknowledged.

REFERENCES

1. Hamad, B.S., Jirsa, J.O., D'Abreu de Palo, N., "Anchorage Strength of Epoxy Coated Hooked Bars," ACI Structural Journal, V. 20, No. 2, March-April 1993, pp. 210-217.

2. Gustafson, D.P., "Epoxy Update," Civil Engineering, ASCE, V. 58, No. 10, October 1988, pp. 38-41.

3. Darwin, D., McCabe, S.L., Hadje-Ghaffari, H., Choi, O.C., "Bond Strength of Epoxy Coated Reinforcement to Concrete - An Update," Serviceability and Durability in Construction Materials, Proceedings of the First Materials Engineering Congress, Denver, CO, August 1990, pp. 115-124.

4. Hadje-Ghaffari, H., Darwin, D., and McCabe, S., "Effects of Epoxy-Coating on the Bond of Reinforcing Steel to Concrete," SM Report No. 28, The University of Kansas Center for Research, July 1991.

5. Ballinger, C.A., "Development of Composites for Civil Engineering," Proceedings of the Conference on Advanced Composite Materials in Civil Engineering Structures, ASCE, Las Vegas, Nevada, 1991, pp. 288-301.

6. Saadatmanesh, H, and Ehsani, M.R., "Application of Fiber-Composites in Civil Engineering," Structural Materials, Proceedings, Structures Congress 1989, ASCE, San Francisco, May 1989 (Orofino, J.F., ed.), pp. 526-535.

7. Sen, R., Iyer, S., Issa, M., and Shahawy, M., "Fiberglass Pretensioned Piles for Marine Environment," Proceedings of the Conference on Advanced Composite Materials in Civil Engineering Structures, ASCE, Las Vegas, Nevada, 1991, pp. 348-359.

8. Wolff, R., and Miesseler, H-J., "New Materials for Prestressing and Monitoring Heavy Structures," Concrete International, V. 11, No. 9, September 1989, pp. 86-89.

9. Dolan, C.W., "Developments in Non-Metallic Prestressing Tendons," PCI Journal, September-October 1990, pp. 80-88.

10. Miesseler, H.-J., and Wolff, R., "Experience with Fiber Composite Materials and Monitoring with Optical Fiber Sensors," Proceedings of the Conference on Advanced Composite Materials in Civil Engineering Structures, ASCE, Las Vegas, Nevada, 1991, pp. 167-181.

11. Goodspeed, C.H., Aleva, G., and Shmeckpeper, E., "Bridge Deck Test Facility for FRP Reinforced Bridge Deck Panels," Use of Composite Materials in Transportation Systems, AMD V. 129, Winter Annual Meeting, ASME, pp. 73-76.

12. Larralde, J., and Siva, R., "Bond Stress-Slip Relationships of FRP Rebars in Concrete," Serviceability and Durability in Construction Materials, Proceedings of the First Materials Engineering Congress, Denver, CO, August 1990, pp. 1134-1141.

13. Iyer, S., and Anigol, M., "Testing and Evaluating Fiberglass, Graphite, and Steel Prestressing Cables for Pretensioned Beams," Proceedings of the Conference on Advanced Composite Materials in Civil Engineering Structures, ASCE, Las Vegas, Nevada, 1991, pp. 44-56.

14. Pleimann, L.G., "Strength, Modulus of Elasticity, and Bond of Deformed FRP Rods," Proceedings of the Conference on Advanced Composite Materials in Civil Engineering Structures, ASCE, Las Vegas, Nevada, 1991, pp. 99-110.

15. Tao, S., Ehsani, M.R., Saadatmanesh, H., "Bond Strength of Straight GFRP Rebars," Materials Performance and Prevention of Deficiencies and Failures, Proceedings of the Materials Engineering Congress, ASCE, Atlanta, GA, 1992, pp. 598-605.

16. Challal, O., Benmokrane, B., "Pullout and Bond of Glass-Fibre Rods embedded in Concrete and Cement Grout," Materials and Structures, V. 26, April 1993, pp. 167-175.

17. Challal, O., Benmokrane, B., "Glass-Fiber Reinforcing Rod: Characterization and Application to Concrete Structures and Grouted Anchors," Materials Performance and Prevention of Deficiencies and Failures, Proceedings of the Materials Engineering Congress, ASCE, Atlanta, GA, 1992, pp. 606-617.

18. Challal, O., Benmokrane, B., Masmoudi, R., "An Innovative Glass-Fire Composite Rebar for Concrete Structures," Advanced Composite Materials in Bridges and Structures, First International Conference, Sherbrooke, Quebec, Canada, 1992, pp. 169-177.

19. Daniali, S., "Development Length for Fibre-Reinforced Plastic Bars," Advanced Composite Materials in Bridges and Structures, First International Conference, Sherbrooke, Quebec, Canada, 1992, pp. 179-188.

20. Ballinger, C., "Structural FRP Composites," Civil Engineering, ASCE, Vol. 60, No. 7, July 1990, pp. 63-65.

21. Tarricone, P., "Plastic Potential," Civil Engineering, Vol. 63, No. 8, August 1993, pp. 62-63.

22. ASTM A 615-89, "Standard Specification for Deformed and Plain Billet-Steel Bars for Concrete Reinforcement," Annual Book of ASTM Standards, Vol. 01.04, 1990.

23. ASTM D 3916-84, "Test Method for Tensile Properties of Pultruded Glass-Fiber-Reinforced Plastic Rod," Annual Book of ASTM Standards, Vol. 08.03, 1991.

24. ASTM D 638-90, "Test Method for Tensile Properties of Plastics," Annual Book of ASTM Standards, Vol. 08.01, 1991.

25. Malvar, L.J., "Confinement Stress Dependent Bond Behavior, Part I: Experimental Investigation," Bond in Concrete, Proceedings of the International Conference, Riga, Latvia, October 1992, pp. 1/79-1/88.

26. Malvar, L.J., "Bond of Reinforcement under Controlled Confinement," ACI Materials Journal, Vol. 89, No.6, November-December 1992, pp. 593-601.

27. Malvar, L.J., "Bond of Reinforcement under Controlled Radial Pressure," Studi e Ricerche, V. 13-1992, Structural Engineering Department, Polytechnic University of Milan, Milan, Italy, 1992, pp. 83-118.

28. Cox, J.V., and Herrmann, L.R., "A Plasticity Model for the Bond Between Matrix and Reinforcement," Proceedings, 6th U.S.-Japan Conference on Composite Materials, Orlando, FL, June 1992.

29. Cox, J.V., Herrmann, L.R., "Confinement Stress Dependent Bond Behavior, Part II: A Two Degree of Freedom Plasticity Model," Bond in Concrete, Proceedings of the International Conference, Riga, Latvia, October 1992, pp. 11/11-11/20.

30. Cox, J.V., "Development of a Plasticity Bond Model for Reinforced Concrete - Theory and Validation for Monotonic Applications," PhD Thesis, University of California, Davis, 1994 (in preparation).

31. Saidpour, S.H., "The Effect of Fibre/Matrix Interfacial Interactions on the Mechanical Properties of Unidirectional E-Glass Reinforced Vinyl Ester Composites," Ph.D. Thesis, Loughborough University of Technology, U.K., 1991.

32. DNV Industrial Services, Tensile Test Results on Nominal 3/4 inch FRP Rebar, 1988.

33. Malvar, L.J., "Bond Stress-Slip Characteristics of FRP Rebars," Technical Report 7058TR, Naval Facilities Engineering Service Center, Port Hueneme, CA 93043, December 1993.

34. Ngo, D., Scordelis, A.C., "Finite Element Analysis of Reinforced Concrete Beams," Journal of the American Concrete Institute, Vol. 64, No. 3, pp. 152-163, 1967.

TABLE 1 - GEOMETRICAL PROPERTIES

Bar Type (3/4" diameter)	Deformation or Indentation Spacing (in)*	Deformation Height or Indentation Depth (in)*
A	0.72 (0.96 ∅) ± 13.8%	0.041 (0.054 ∅) ± 7.5%
B	0.94 (1.25 ∅) ± 1.9%	0.063 (0.084 ∅) ± 51.8%
C	0.78 (1.03 ∅) ± 2.3%	0.047 (0.067 ∅) ± 2.8%
D	1.35 (1.80 ∅) ± 7.6%	0.069 (0.092 ∅) ± 13.7%
Steel	< 0.525 (0.70 ∅)	> 0.038 (0.0507 ∅)

* 1" = 25.4 mm

TABLE 2 - MECHANICAL PROPERTIES

Bar Type	Test Procedure	Number of Tests	Modulus of Elasticity (Msi)*	Ultimate Stress (Ksi)+	Ultimate Strain (%)
A	ASTM D3916-84	5	6.74 (± 1.3%)	86.7 (± 2.2%)	1.41 (± 3.4%)
A	Special grips	3	-	89.5 (± 2.7%)	-
B	ASTM D3916-84	5	4.10 (± 22.6%)	65.1 (± 20.7%)	1.73 (± 11.2%)
C	ASTM D3916-84	5	6.88 (± 2.4%)	81.4 (± 5.1%)	1.23 (± 6.5%)
C	Special grips	3	-	103.0 (± 5.1%)	-
D	ASTM D3916-84	5	5.77 (± 2.2%)	81.3 (± 2.2%)	1.79 (± 3.8%)

* 1 Msi = 6.9 GPa
+ 1 Ksi = 6.9 MPa

TABLE 3 - ANALYTICAL FIT PARAMETERS

BAR TYPE	A	B	C	D	E	F	G
Type A	1.00	9.04	0.05	0.0270	0.00317	11.0	1.1
Type D	0.266	5.63	0.15	0.0633	0.02824	13.0	0.5
Steel 68° lugs	0.9	3.5	0.35	0.0279	0.00508	9.0	0.65
Steel 90° lugs	0.9	4.4	0.35	0.0071	0.00770	5.5	1.1

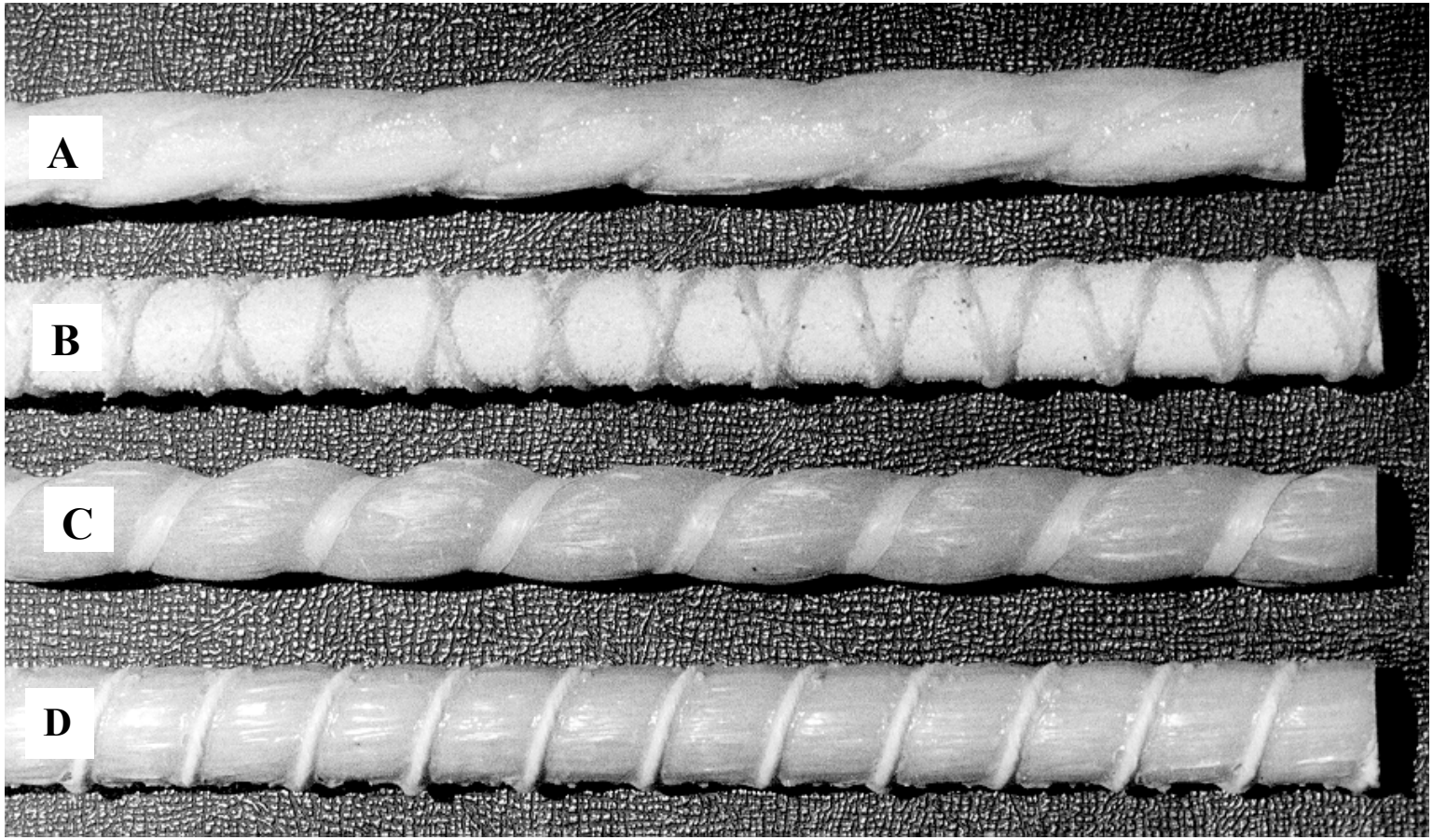

Figure 1. Bar types.

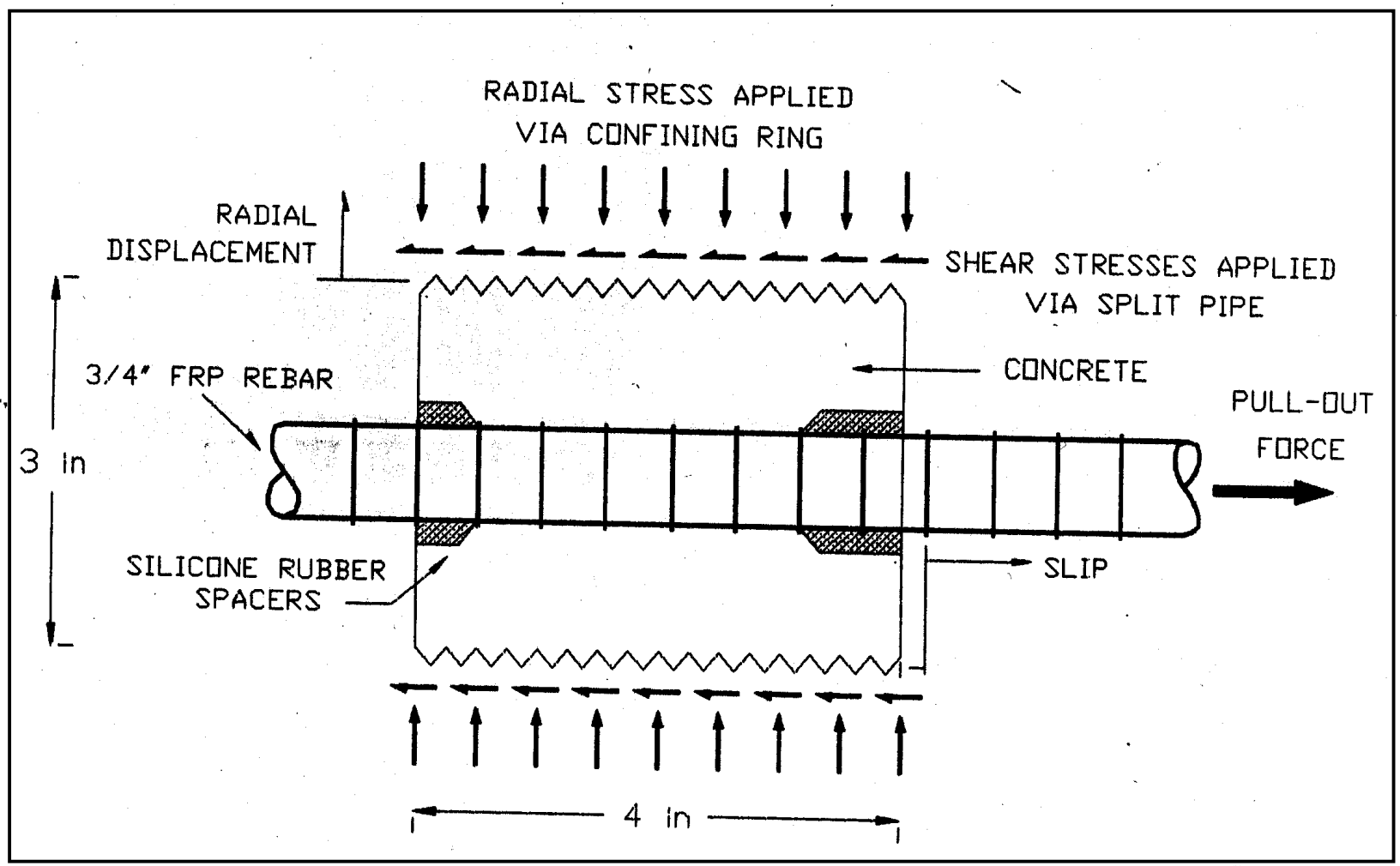

Figure 2. Test specimen (1 inch = 25.4 mm).

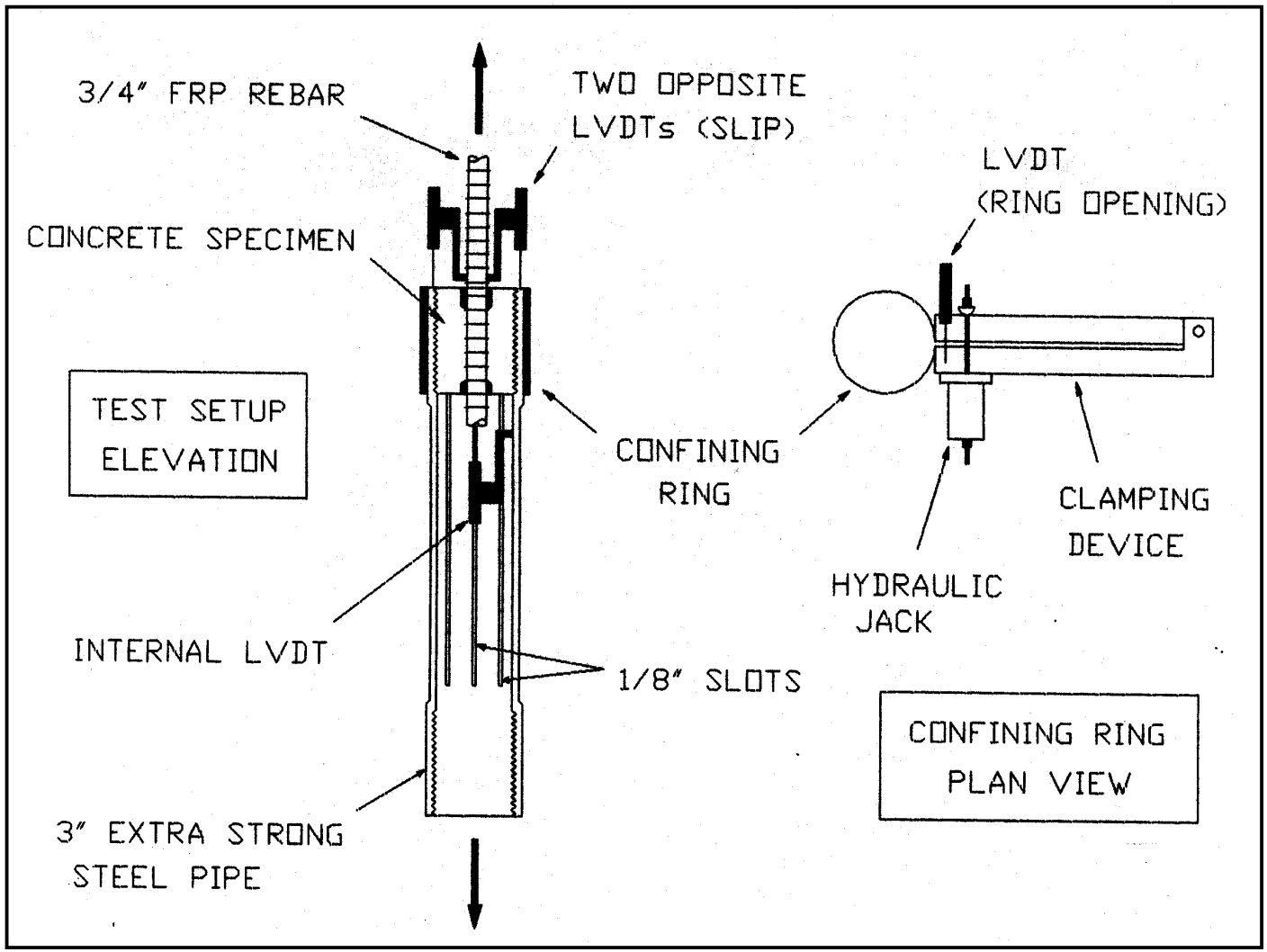

Figure 3a. Schematic of bond tests set up (1 inch = 25.4 mm).

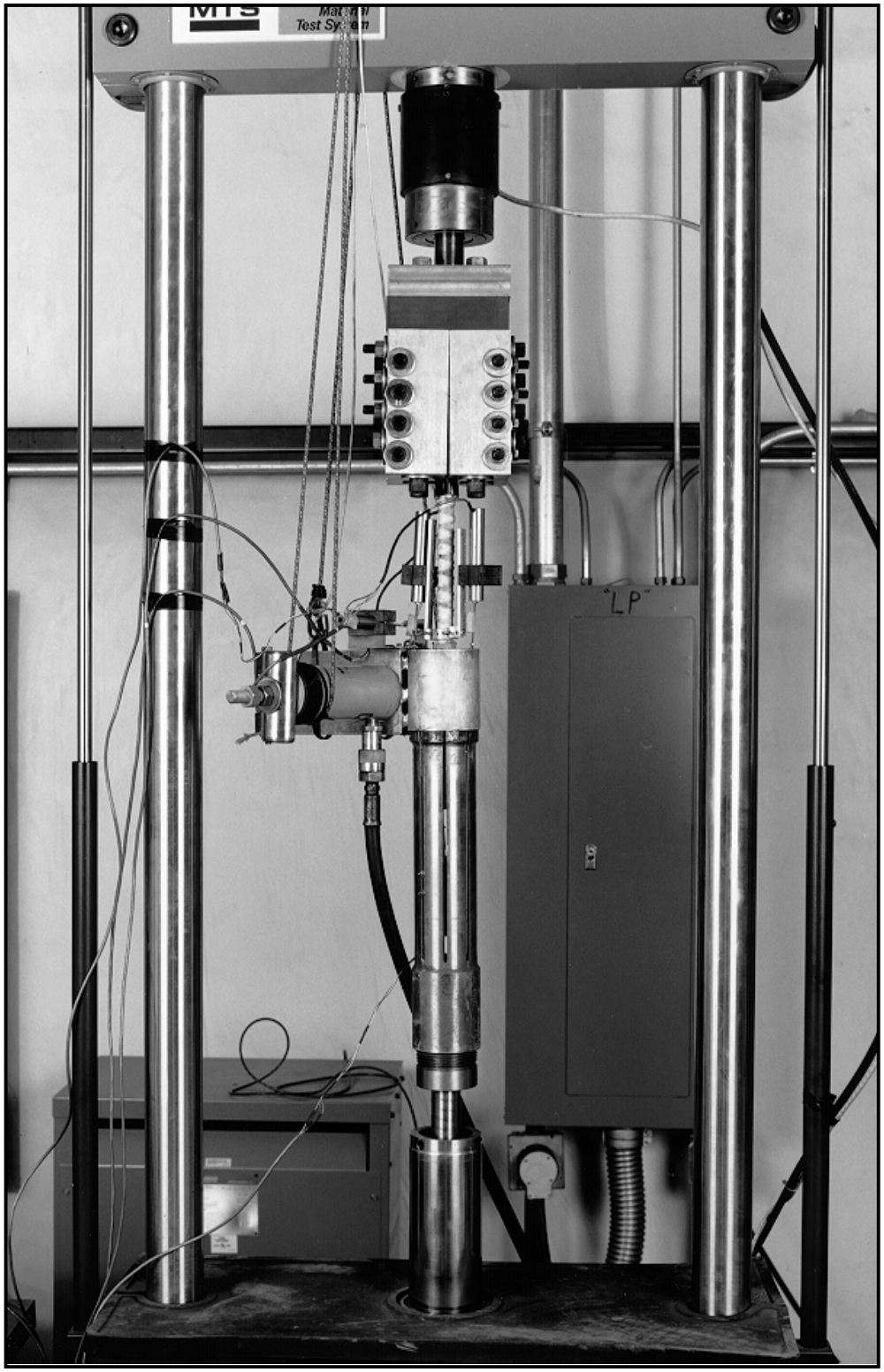

Figure 3b. Bond tests set up.

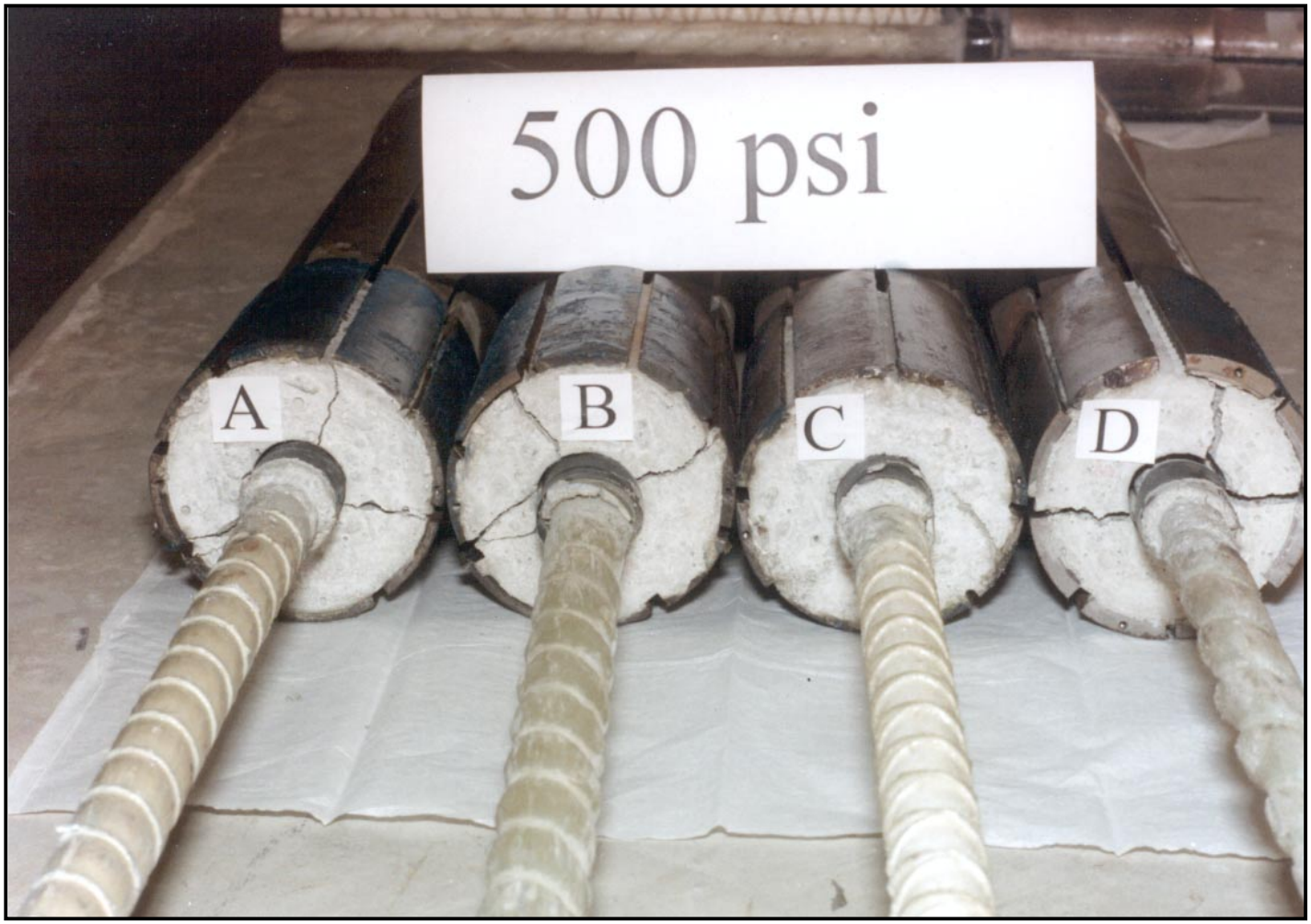

Figure 4. Longitudinal cracks.

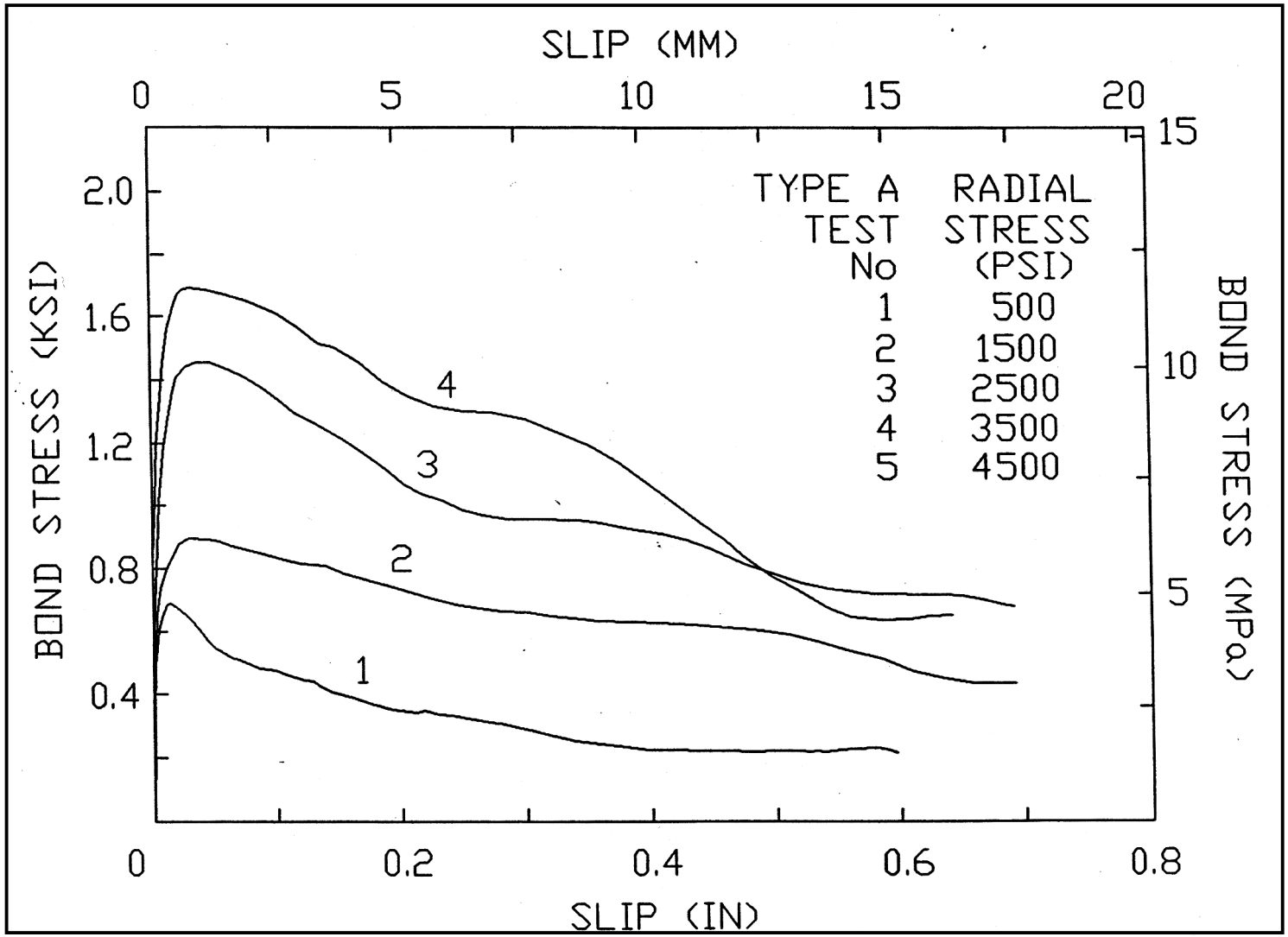

Figure 5a. Complete bond stress-slip curves, type A.

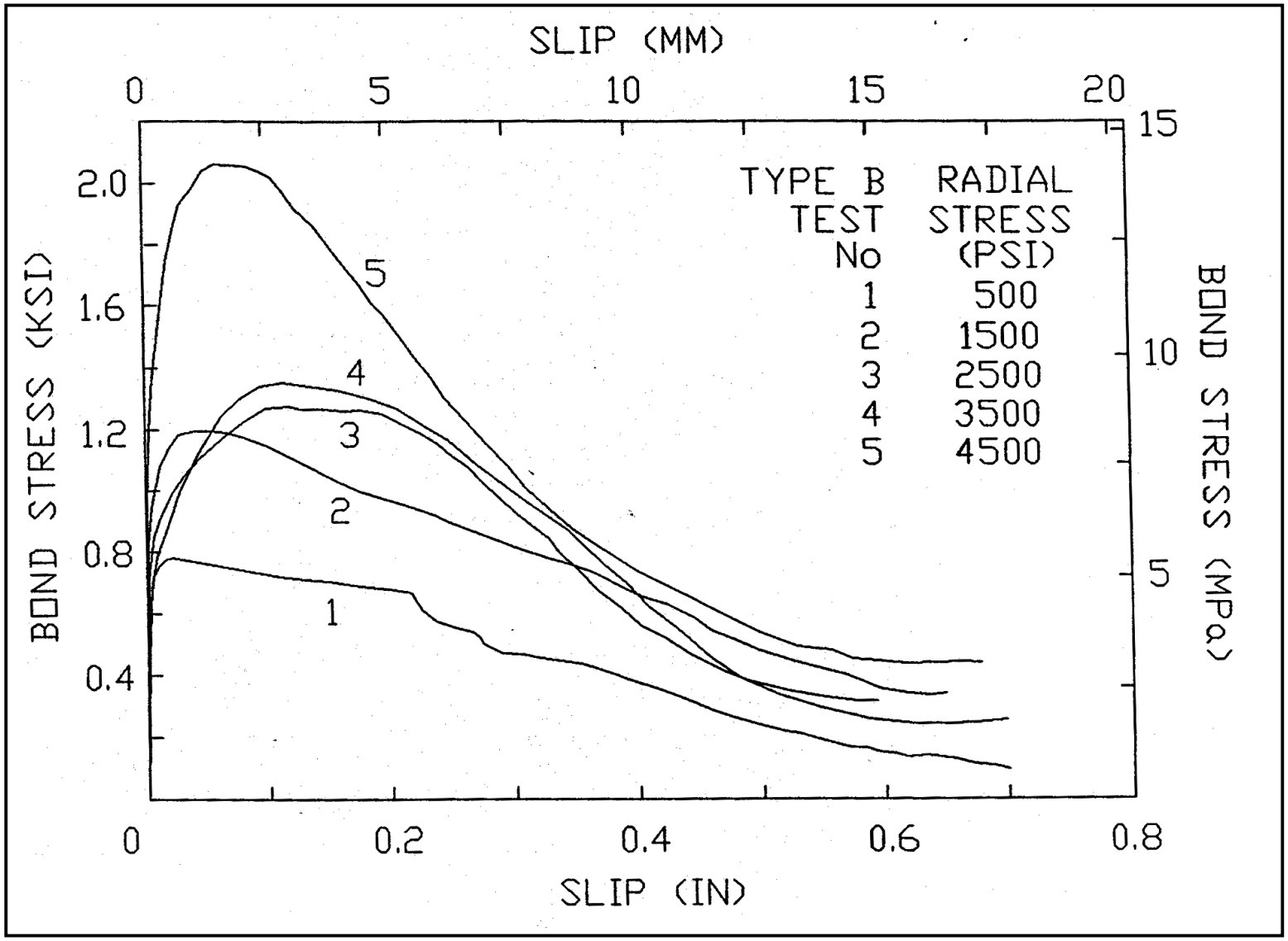

Figure 5b. Complete bond stress-slip curves, type B.

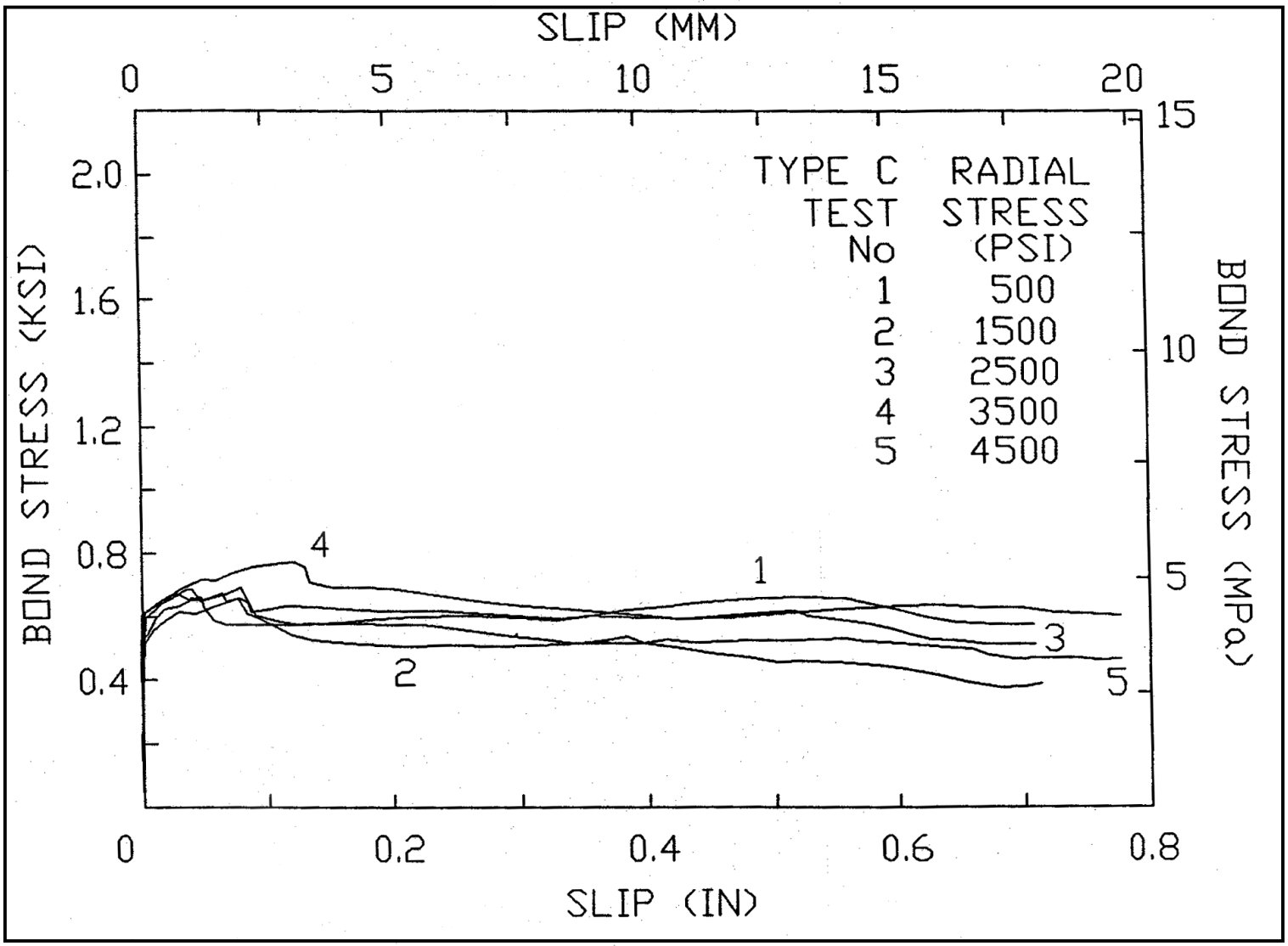

Figure 5c. Complete bond stress-slip curves, type C.

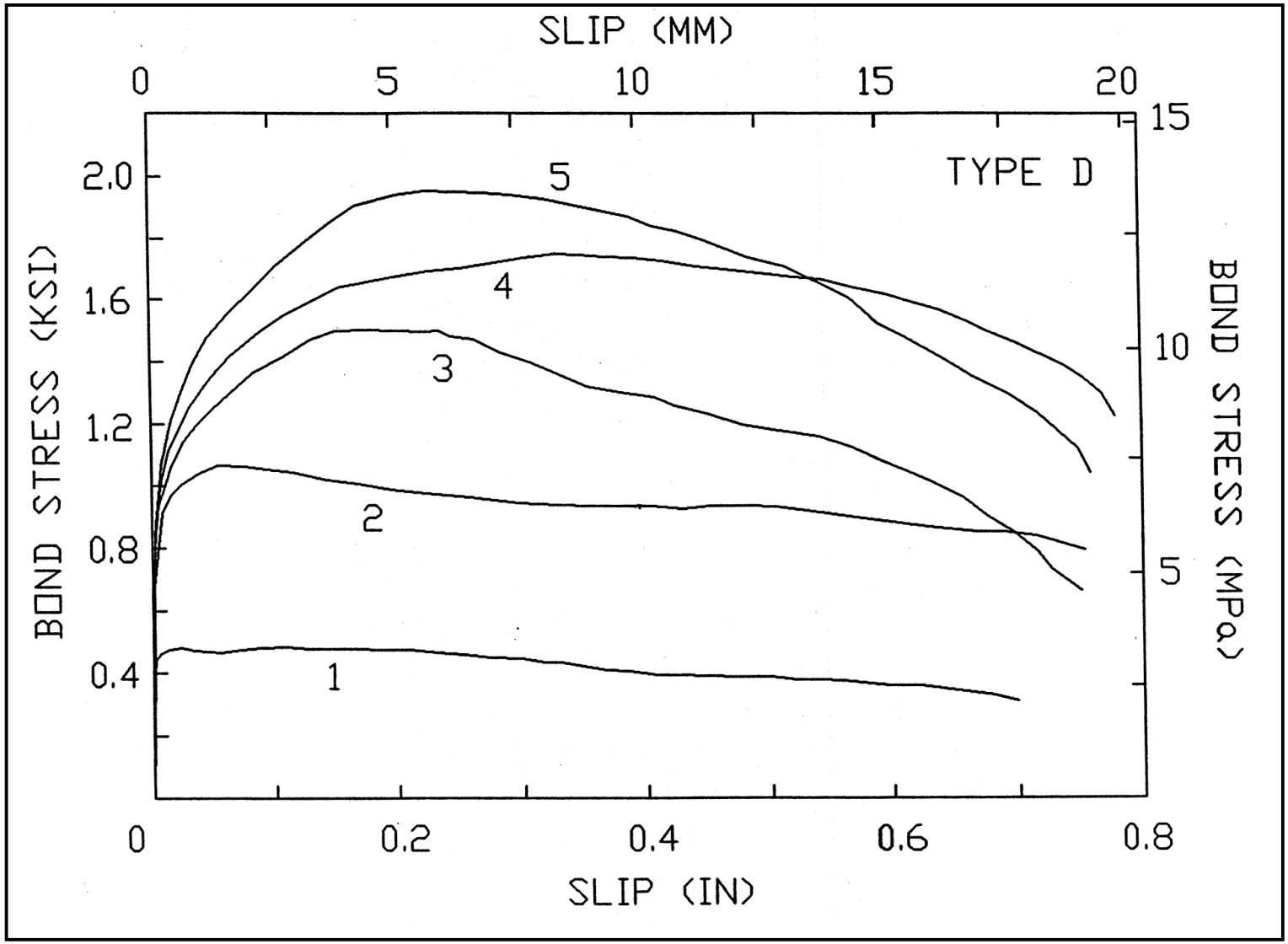

Figure 5d. Complete bond stress-slip curves, type D.

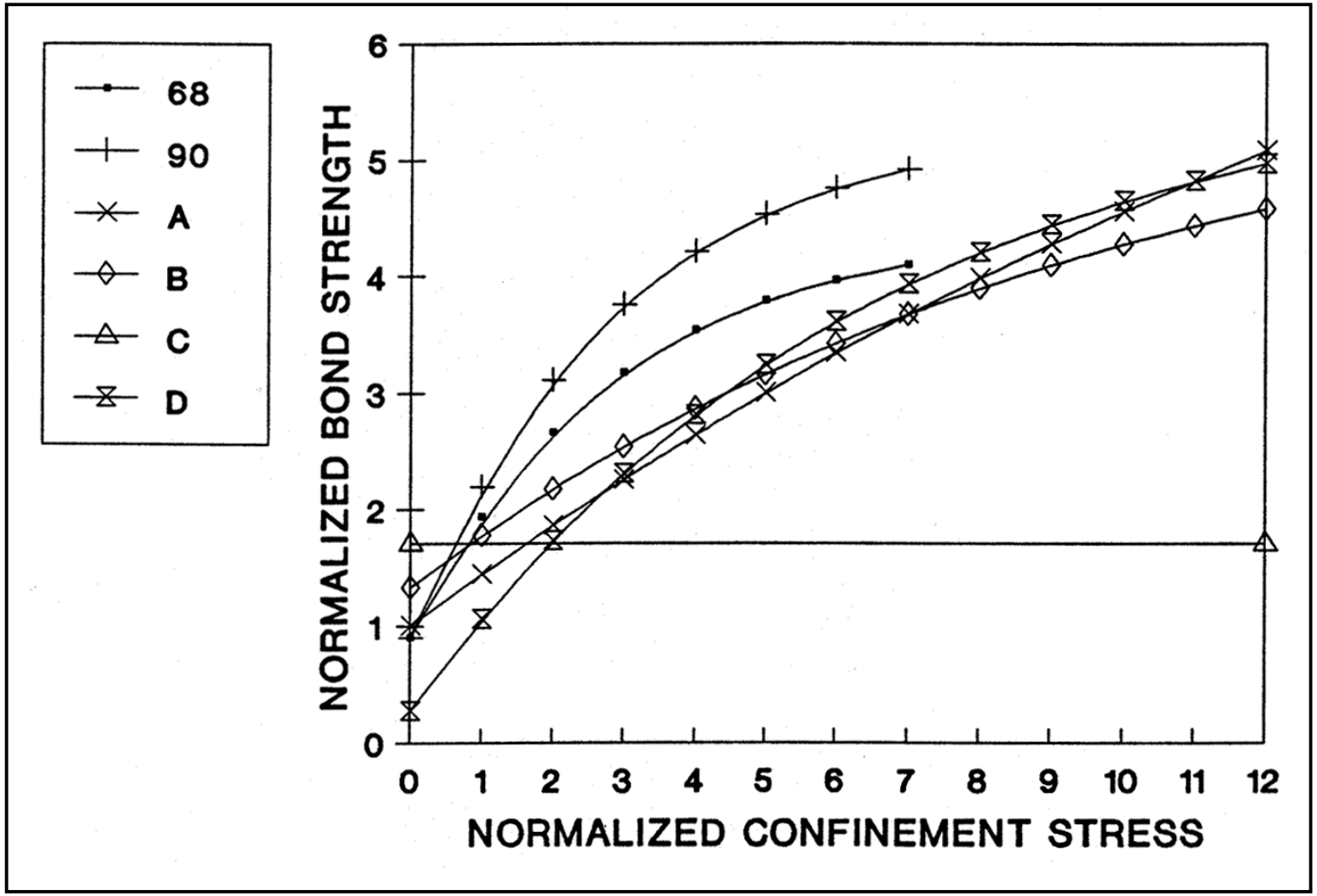

Figure 6. Bond strength: Comparison to previous steel results.

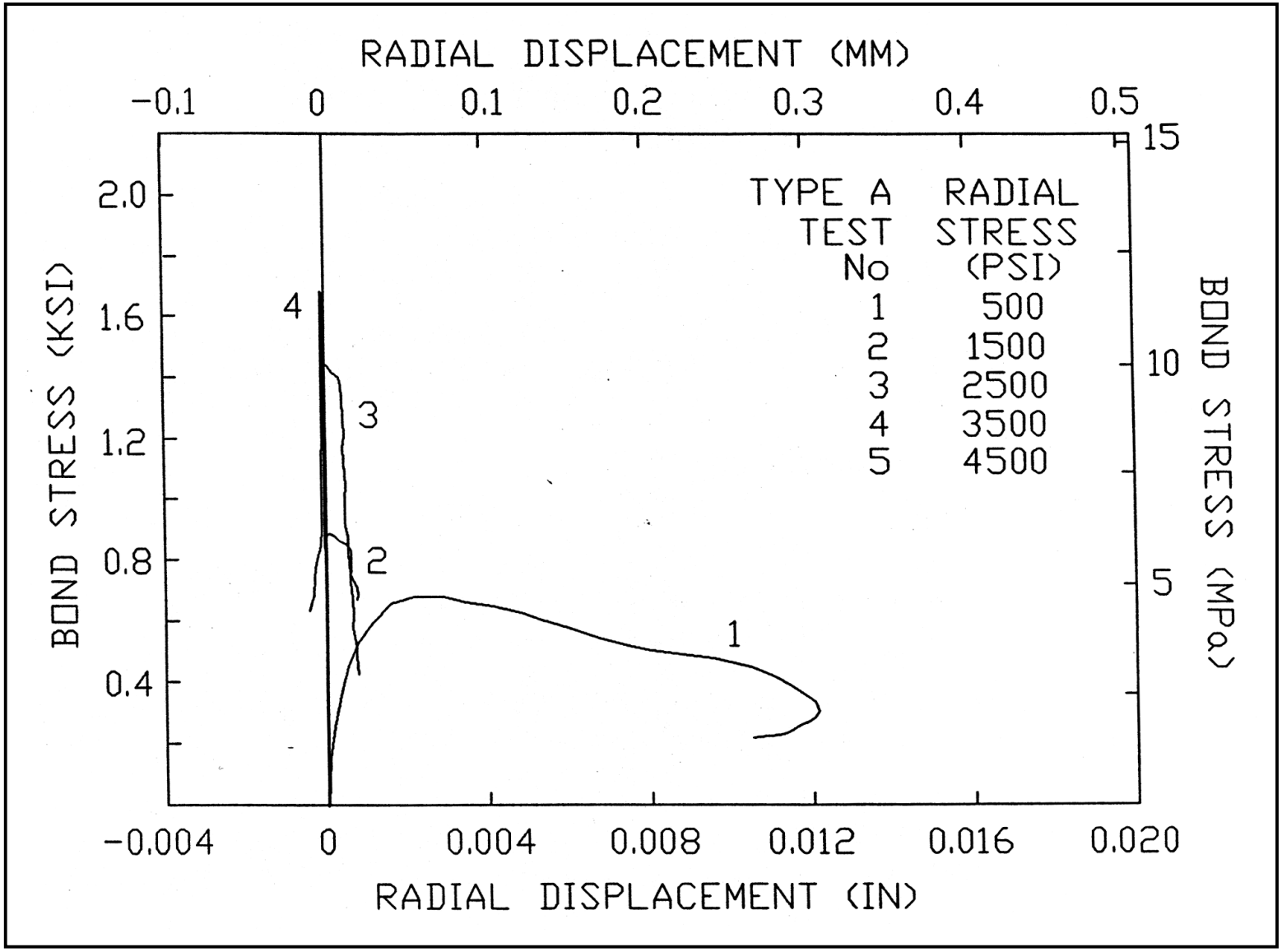

Figure 7a. Bond stress-radial displacement curves, type A.

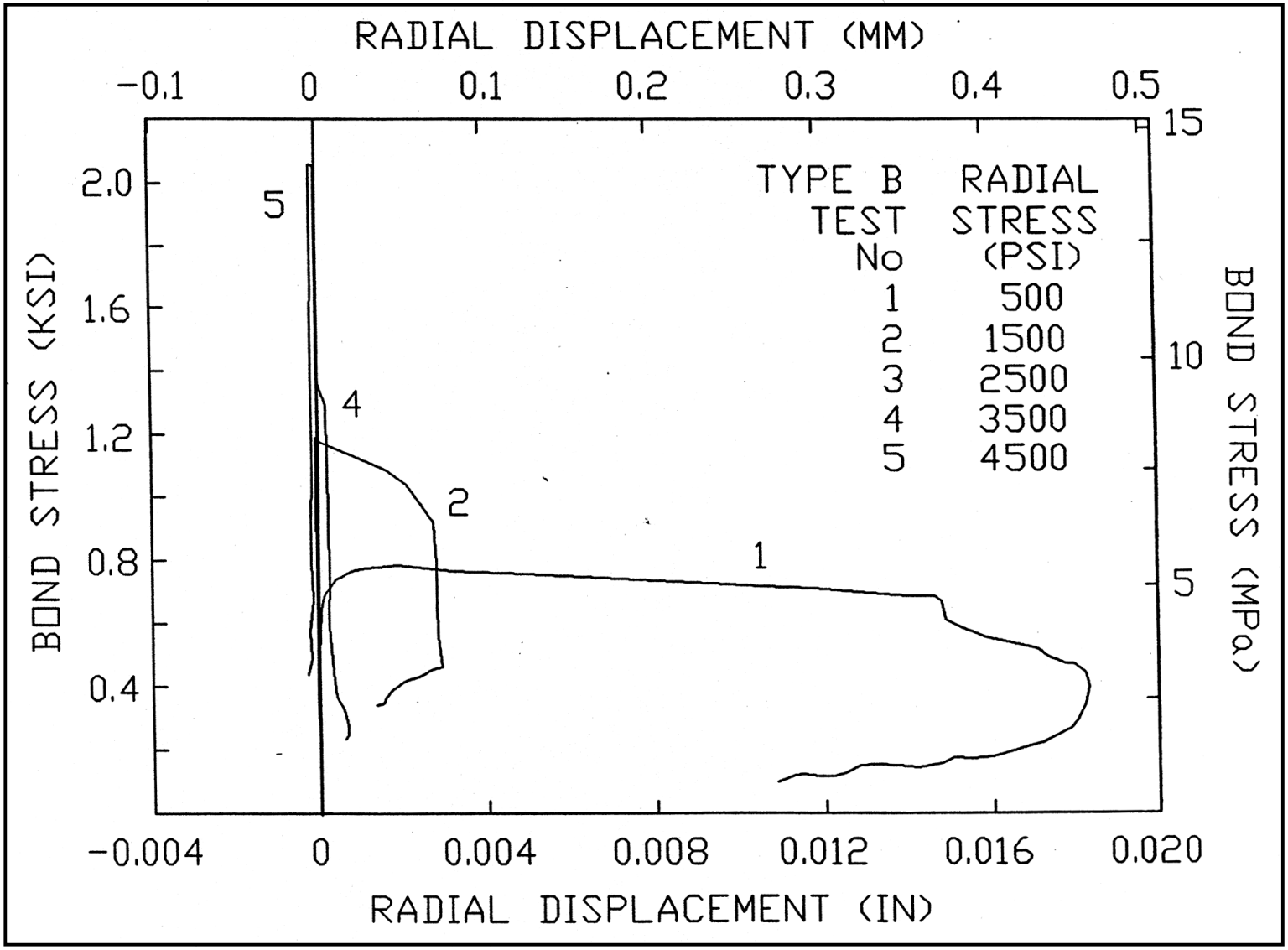

Figure 7b. Bond stress-radial displacement curves, type B.

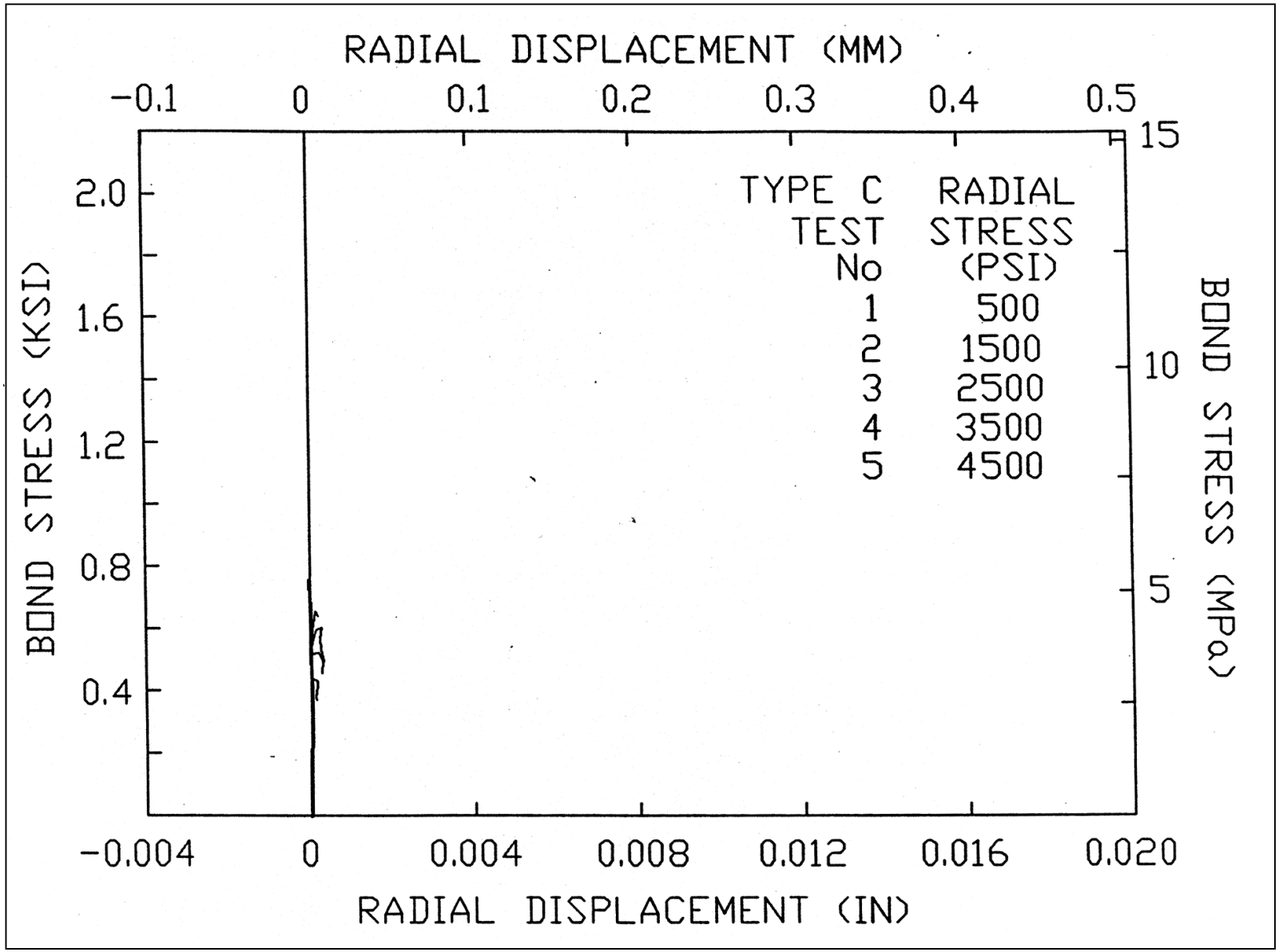

Figure 7c. Bond stress-radial displacement curves, type C.

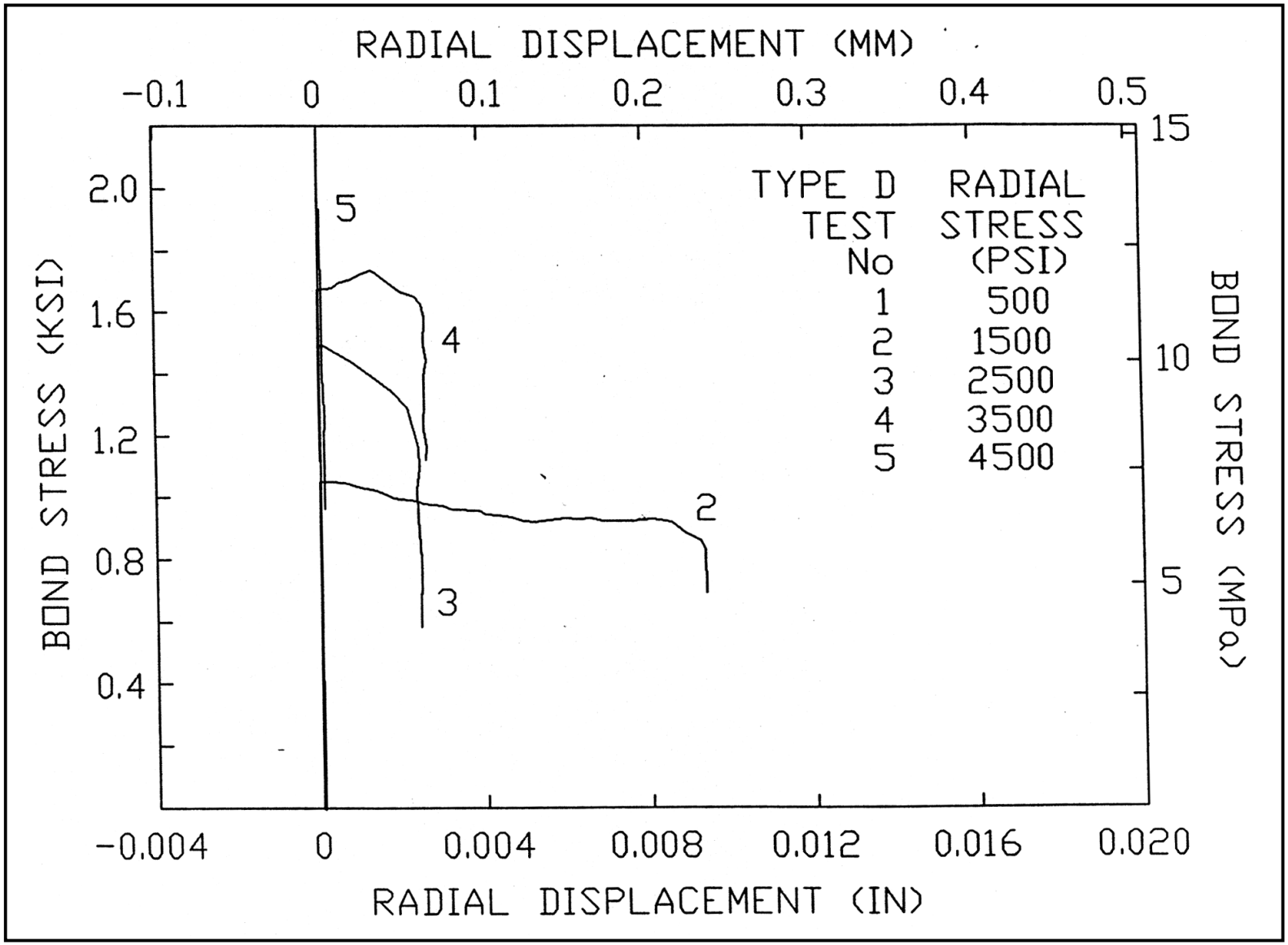

Figure 7d. Bond stress-radial displacement curves, type D.

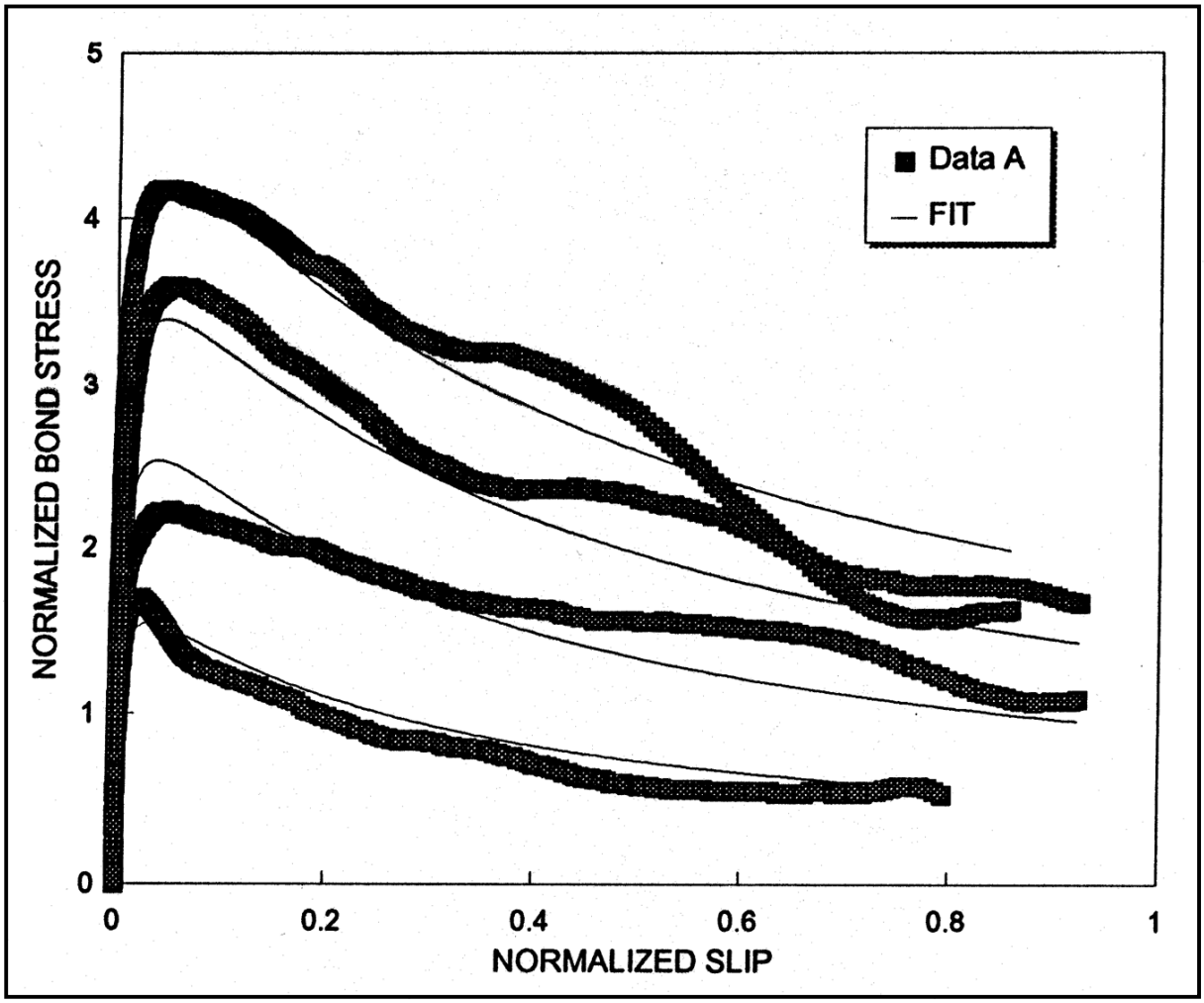

Figure 8. Fit of type A bond stress-slip data.